Chapter 6

GRB 050319 : Wind to ISM Transition

Abstract

The collapse of a massive star is believed to be the most probable progenitor of a long GRB. Such a star is expected to modify its environment by stellar wind. The effect of such a circum-stellar wind medium is expected to be seen in the evolution of a GRB afterglow, but has so far not been conclusively found. We claim that a signature of wind to constant density medium transition of circum-burst medium is visible in the afterglow of GRB 050319. Along with the optical observations of the afterglow of GRB 050319 we present a model for the multiband afterglow of GRB 050319. We show that the break seen in optical light curve at ~ 0.02 day could be explained as being due to wind to constant density medium transition of circum-burst medium, in which case, to our knowledge, this could be the first ever detection of such a transition at any given frequency band. Detection of such a transition could also serve as a confirmation of massive star collapse scenario for GRB progenitors, independent of supernova signatures.

6.1 Introduction

One of the long standing questions in astrophysics is the progenitors of Gamma Ray Bursts (GRBs). Collapse of a massive star is one of the most favoured progenitors of the long GRBs. Evidence for a massive star being a GRB progenitor may be obtained in two different ways, both using observations of GRB afterglows. *(1) Supernova (SN) component underlying the GRB afterglow* : A few of the nearby GRB afterglows have shown the temporal and spectroscopic signature of an underlying SN. see e.g., (Stanek et al., 2003) *(2) Evolution of GRB afterglow in the stellar wind medium* : Massive stars modify the density profile of the circum-stellar medium due to the powerful winds they drive during their life time. For a constant mass loss rate and constant wind velocity the circum-burst medium assumes a density profile $\rho \propto r^{-2}$ as compared to ρ = constant in the absence of stellar wind. Evolution of the GRB afterglow light curves is significantly different in these two cases of density profiles (Wijers and Galama, 1999; Chevalier and Li, 2000). Attempts to look for the signatures of such a wind-modified circum-burst density profile in the light curves of GRB afterglows have not been conclusive so far. In the case of GRB 050904 Gendre et al. (2007) find that the early x-ray afterglow suggests a wind-like density profile of the circum-burst medium while the late optical afterglow was consistent with evolution in a constant density medium. Hence, they conjecture that a transition between these two types of density profiles would have taken place somewhere in between. However, this transition was not directly observed in the light curve of any given band. In this chapter, we present observations of the afterglow of GRB 050319 and use these observations along with those available in the literature to model the light curve evolution as being due to the transition of circum-burst medium from wind-like to constant density medium.

In the next section, we give a brief introduction about GRB 050319 and

present our observations of its afterglow. In § 6.3 we present a preliminary analysis of the afterglow light curves to understand their multi-wavelength behaviour. Our inferences about the circum-burst density profile drawn from the preliminary analysis and then by using the numerical fits to the afterglow light curves are prsented in § 6.4. The resulting physical parameters for GRB 050319 are discussed in § 6.4.1. § 6.5 is devoted to the discussion of stellar wind bubbles and circum-stellar density profile (§ 6.5.1), non-detection of winds in GRB afterglows and possible astrophysical scenarios for it (§ 6.5.2). Implications of our results for the models of GRB progenitors are discussed in § 6.5.3. Our conclusions are summarised in § 6.6.

6.2 Observations and Data Reduction

GRB 050319 was detected by the Burst Alert Telescope (BAT) instrument of the SWIFT satellite on 2005 March 19, 09:31:18.44 UT (Krimm et al., 2005b,a). However, Cusumano et al. (2006), using the re-analysis of the BAT data, pointed out that *Swift* was slewing during the GRB onset and the BAT trigger was switched off. The GRB was recognised about 135 seconds after its actual onset. The total duration of the GRB (T_{90}) was thus 149.7 s (Cusumano et al., 2006) instead of 10 ± 2 s (Krimm et al., 2005b,a). The burst fluence in 15-350 keV band within the T_{90} duration is estimated to be 1.6×10^{-6} erg cm^{-2}. The photon index of the time-averaged single power law spectrum is 2.1 ± 0.2. *Swift* XRT and UVOT located a bright source at $\alpha = 10^{h}16^{m}48^{s}$ and $\delta = +43°32'47''$ (J2000) which was later confirmed by Rykoff et al. (2005) with ROTSE-IIIb. Fynbo et al. (2005) obtained the spectra of the afterglow of GRB 050319 on 2005 March 20 and the redshift of the afterglow was measured to be $z = 3.24$. At this redshift, the gamma ray isotropic equivalent energy released during the burst is 3.7×10^{52} erg for a flat universe with $\Omega_m = 0.3, \Omega_\Lambda = 0.7$ and $H_0 = 70$ km s^{-1} Mpc^{-1}.

Optical CCD observations of the afterglow of GRB 050319 were carried out in Johnson BV and Cousins RI filters using the 104-cm Sampurnanand Telescope of ARIES, Nainital with regular specifications of the CCD camera and using standard observation procedures of bias subtraction and flat fielding. For details of the telescope and detector systems see Chapter 3 of this thesis. The standard procedure of observation and data reduction is also presented in Chapter 3 of this thesis.

Henden (2005) has presented a photometry of the GRB field. We calibrated the BVRI magnitudes of the optical transient (OT) differentially using secondary stars numbered 8, 9, 10, 11 and 13 in the list of Henden (2005). The magnitudes derived in this way are listed in Table 6.1 and the secondary stars are shown in Figure 6.1. The photometric magnitudes available in the literature by Woźniak et al. (2005); Quimby et al. (2006); Mason et al. (2006) were converted to the present photometric scales using the five secondary stars mentioned above.

6.3 Light curves of GRB 050319

Along with our own observations we have used observations reported in the literature to study the light curves of GRB 050319 afterglow. The x-ray afterglow was observed by *Swift* XRT starting from $\sim$ 220s to 28 days (Cusumano et al., 2006) after the burst. Attempts to observe the afterglow at radio wavebands resulted in upper limits (Soderberg, 2005a,b; Volvach and Pozanenko, 2005). The optical afterglow was observed by Woźniak et al. (2005); Quimby et al. (2006); Mason et al. (2006) resulting in a coverage from a few seconds to ~ 4 days after the burst.

To construct the optical light curve we have corrected the observed magnitudes for the standard Galactic extinction law given by Mathis (1990). The galactic extinction in the direction of GRB 050319 is estimated to be E(B-V) = 0.011 mag from the smoothed reddening map provided by Schlegel et al. (1998). The effective

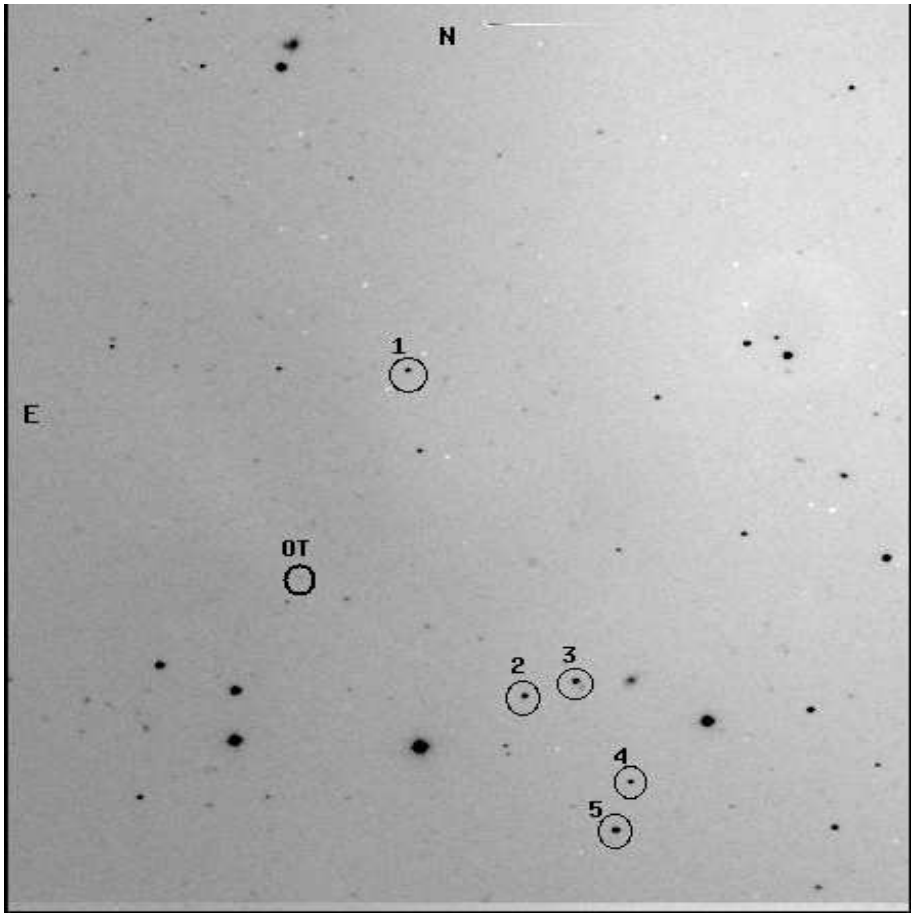

Figure 6.1: R band image of GRB 050319 optical afterglow obtained using the 104-cm ST at ARIES, Nainital. The position of the optical afterglow is marked with a circle. Also marked are the comparison stars from Henden (2005). North is up and East is to the left.

Date (UT) 2005 March	Magnitude (mag)	Exposure Time (s)	Passband
19.7512	21.02±0.14	2×900	B
19.7457	20.23±0.20	600	V
19.8558	20.60±0.21	600	V
19.6949	19.46±0.16	300	R
19.6999	19.25±0.10	300	R
19.7215	19.98±0.11	300	R
19.7539	20.06±0.13	300	R
19.7874	20.03±0.16	300	R
19.7129	19.59±0.19	300	I
19.7587	19.66±0.25	300	I

Table 6.1: CCD BVRI broad band optical observations of the GRB 050319 afterglow using the 104-cm Sampurnanand Telescope at ARIES, Nainital.

wavelength and normalization given by Bessell et al. (1998) were used to convert the magnitudes to fluxes in μJy.

Most of the GRB afterglow light curves are well characterized by a broken power law of the form $F = F_0\{(t/t_b)^{\alpha_1 s}+(t/t_b)^{\alpha_2 s}\}^{-1/s}$ where α_1 and α_2 are the afterglow flux decay indices before and after the break time (t_b), respectively. F_0 is the flux normalization and 's' is a smoothening parameter which controls the sharpness of the break. Most known GRB afterglows have $\alpha_2 > \alpha_1$ i.e. the decay becomes steeper after the break. Interestingly, the optical afterglow light curve of GRB 050319 shows steeper to flatter decay with a break at $\sim$ 0.02 day. This behavior

of light curve decay is difficult to explain using the fireball model which assumes a relativistic shock wave propagating into medium having either uniform density profile or wind density profile. The x-ray and optical light curves also show some variability superimposed on the power law decay. The x-ray light curve shows a break near ~ 0.3 day. We quantify the various characteristics of the afterglow light curves as summarized below.

1. The x-ray afterglow of GRB 050319 shows a very rapid decay before ~ 0.005 day (~ 384 s) after the GRB. The decay then flattens before steepening again at ~ 0.3 day. Cusumano et al. (2006) has characterised the afterglow into three separate temporal evolutions in x-ray bands :

$$\alpha_X = \begin{cases} 5.53 \pm 0.67 & (\Delta t < 0.004 \text{ day}); \\ 0.54 \pm 0.04 & (0.004 \text{ day} < \Delta t < 0.3 \text{ day}); \\ 1.14 \pm 0.2 & (\Delta t > 0.3 \text{ day}); \end{cases}$$

2. The B, V and R band light curve also show a rapid decline during the early phase ($\Delta t < 0.02$ day) which flattens at later epochs. Thus, the afterglow can be separated into two separate temporal evolutions in the R band as follows :

$$\alpha_R = \begin{cases} 1.09 \pm 0.03 & (\Delta t < 0.02 \text{ day}); \\ 0.51 \pm 0.03 & (0.02 \text{ day} < \Delta t < 10.0 \text{ day}); \end{cases}$$

And for B, V and I bands we measure following α s :

$$\alpha_B = \begin{cases} 1.46 \pm 0.26 & (\Delta t < 0.02 \text{ day}); \\ 0.33 \pm 0.05 & (0.02 \text{ day} < \Delta t < 1.0 \text{ day}); \end{cases}$$

$$\alpha_V = \begin{cases} 0.90 \pm 0.05 & (\Delta t < 0.02 \text{ day}); \\ 0.50 \pm 0.04 & (0.02 \text{ day} < \Delta t < 1.0 \text{ day}); \end{cases}$$

$$\alpha_I = 0.59 \pm 0.13 \qquad (0.02 \text{ day} < \Delta t < 1.0 \text{ day});$$

The average decay index of the optical light curve, at early and late epochs, is then

$$\alpha_{opt} = \begin{cases} \alpha_1 = 1.15 \pm 0.27 & (\Delta t < 0.02 \text{ day}); \\ \alpha_2 = 0.48 \pm 0.15 & (0.02 \text{ day} < \Delta t < 1.0 \text{ day}); \end{cases}$$

respectively.

6.4 GRB 050319 afterglow : wind or homogeneous density profile ?

The breaks seen in x-ray light curve (at $\sim$ 384 s and at $\sim$ 0.3 day) are not accompanied by simultaneous breaks in optical wavebands. Similarly, the break seen in optical band has no simultaneous counterpart in the x-ray light curve. Also, the sense of slope change, i.e. $\alpha_2 < \alpha_1$, as seen in optical waveband is contrary to the predictions of the fireball model (Sari et al., 1998, 1996) which expects $\alpha_1 < \alpha_2$. Thus, the behaviour of the afterglow of GRB 050319 is different from what has so far been commonly observed in the GRB afterglows.

We propose a different model to explain the afterglow of GRB 050319 as being due to a transition of the circum-burst medium density profile that the explosion generated shock wave is interacting with. In this model, the observed change from steep to flat decay of the optical afterglow of GRB 050319 at 0.02 day could be explained as being due to the change in the density profile of the circum-burst medium from wind modified ($\rho \propto r^{-2}$) to the constant density medium (ρ = constant). The break in the light curve occurs when the shock front interacts with the boundary between the two density profiles. Below we describe and reproduce various features of the GRB 050319 afterglow using this model of 'wind to constant density medium transition'.

The early steep decay of x-ray afterglows ($\alpha \sim 3$ to 5) as is seen in the case of GRB 050319 are now seen routinely in most of the GRBs (Nousek et al., 2006) and has become a canonical feature of the GRB x-ray afterglows. In the case of GRB 050319, Cusumano et al. (2006) conjecture that emission during the phase of early steep decay could be the low energy tail of the GRB prompt emission. We exclude this early emission from the rest of our discussion and we will restrict ourselves to

the rest of the x-ray light curve.

The radiation spectrum of GRB afterglows exhibits a power law spectrum characterised by three break frequencies - the self absorption frequency $\nu_{\rm a}$, the peak frequency $\nu_{\rm m}$ corresponding to the lower cutoff in the electron energy distribution ($n(\gamma) \propto \gamma^{-p}$, $\gamma > \gamma_m$), and the synchrotron cooling frequency $\nu_{\rm c}$. The flux $F_{\rm m}$ at $\nu_{\rm m}$ provides the normalisation of the spectrum (Sari et al., 1998). A detailed discussion about these spectral breaks and the peak flux is provided in Chapter 1 of this thesis.

The photon index (Γ) of the afterglow and the electron energy distribution index p are related in any given spectral regime ($\Gamma - 1 = p/2$ if $\nu > \nu_{\rm c}$ and $\Gamma - 1 = (p-1)/2$ if $\nu < \nu_{\rm c}$). The corresponding temporal decay index α would be $(3p-2)/4$ and $3(p-1)/4$ respectively before the jet break and would equal p in both spectral regimes after the jet break, according to the standard fireball model for an afterglow expanding in a homogeneous interstellar medium (ISM). For the shock wave expanding into the wind density profile, the corresponding α would be $(3p-2)/4$ and $(3p-1)/4$ respectively before the jet break and p after the jet break.

In the present case, the observed values of the photon index ($\Gamma = 1.69 \pm 0.06$) and temporal decay index ($\alpha_{\rm X} = 0.54 \pm 0.04$) of the x-ray afterglow are consistent with the spectral regime $\nu_{\rm X} > \nu_{\rm c}$ and $p = 1.5$. The observed decay indices of optical light curve are also consistent with the inferred value of p, the spectral regime $\nu_{\rm opt} < \nu_{\rm c}$ and wind-constant density transition at 0.02 day. As discussed above, the expected temporal decay index of the x-ray afterglow, $\alpha_{\rm X} = (3p-2)/4$, is the same for wind and homogeneous ISM density profiles. The absence of a break in the x-ray afterglow light curve simultaneous with the optical break makes the multiband afterglow features consistent with the proposed transition of the circum-burst medium density profile from wind to constant density. In Figure 6.2. we compare the predictions of our model of wind to constant density transition of the

circum-burst density profile with multiband observations of GRB 050319 afterglow. A detailed list of the best fit spectral parameters can be found in Table 6.2. The observed B band light curve is systematically lower than that predicted by the model which could be due to the *Lyman* α absorption at $z = 3.24$ appearing in the observer's B band as suggested by Huang et al. (2007). The steepening of the x-ray light curve at $\Delta t \sim 0.3$ day could be due to jet break (Cusumano et al., 2006) but unfortunately the variability in R band light curve and insufficient sampling of the data in B and V bands after ~ 1.0 day makes it difficult to verify the achromaticity of the break.

	wind density medium	constant density medium
$\nu_m(Hz)$	$1.6^{+0.9}_{-0.7} \times 10^{13}$	$1.0^{+0.35}_{-0.5} \times 10^{12}$
$\nu_c(Hz)$	$1.1^{+3.7}_{-0.4} \times 10^{15}$	$2.1^{+0.6}_{-0.8} \times 10^{15}$
$F_{peak}(\mu Jy)$	2370 ± 355	1810^{+260}_{-170}
p	1.59 ± 0.06	1.52 ± 0.02
$\chi^2_{dof}(dof)$	1.4 (161)	

Table 6.2: The best fit spectral parameters for wind (< 0.02 day) and constant density (> 0.02 day) profile. All the parameters are fitted at 0.003 day after the burst.

Given the above model spectral parameters we find that the broadband behavior of the afterglow is very well explained. However, we are restricting ourselves to the overall behavior of the afterglow and hence do not attempt in our model to reproduce the variations seen in the optical light curve. The reason for these variations could be density inhomogeneities in the circum-burst medium.

6.4.1 Physical Parameters

Four spectral parameters (ν_a, ν_m, ν_c and F_{peak}) are related to four physical parameters viz n (no density of the constant density circum-burst medium) or A_* (defined as

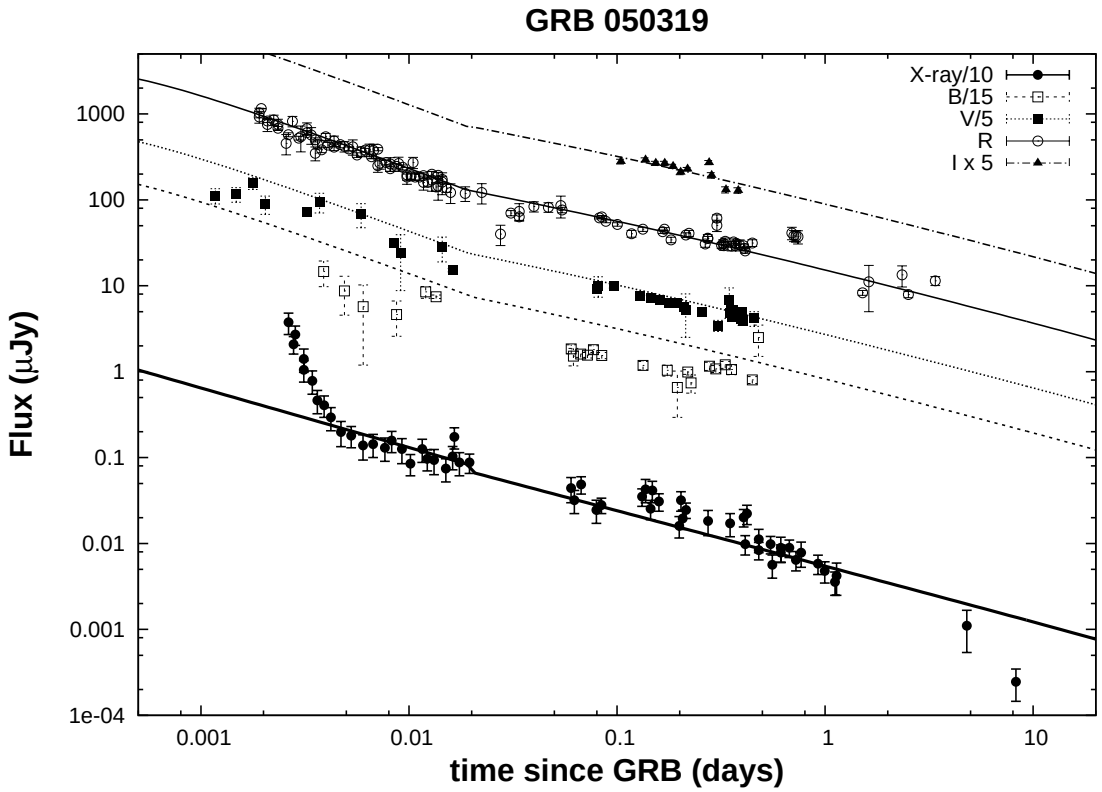

Figure 6.2: The afterglow light curves of GRB 050319. The solid lines represent a model in which the expanding fireball encounters the transition in density profile from the wind to constant density medium at 0.02 day. The best fit spectral parameters of this model are listed in Table 6.2

$\rho(r) = 5 \times 10^{11} A_* r^{-2}$ for wind density medium), E (total energy content of the fireball), energy fraction in relativistic electrons ϵ_e and that in magnetic field ϵ_B. The typical value of self absorption frequency ν_a lies in radio-mm waves and hence is best estimated only if the afterglow is well observed in these bands. Unfortunately, the afterglow of GRB 050319 was never detected at the radio band (Soderberg, 2005a,b; Volvach and Pozanenko, 2005). Therefore we expressed the remaining three spectral parameters, known separately from parts of the light curves corresponding to the wind and the constant density circum-burst medium, in terms of A_* and n, respectively. Equating the kinetic energies estimated from two density profiles, i.e.

$E^K_{wind} = E^K_{ISM}$, we obtain a relation between A_* and n : $A_* = 5.097 \times 10^{-3}\ n^{2/5}$. For a typical range of values of n (1 to 100), estimated A_* ranges from 5.097×10^{-3} to 0.032 which results in the range of E^K_{iso} from 1.3×10^{54} to 5.3×10^{53} erg. All the estimated physical parameters are listed in Table 6.3.

Parameter	n = 1; $A_* = 5.097 \times 10^{-3}$		n = 100; $A_* = 0.032$	
	wind	ISM	wind	ISM
E^{iso}_{54}	1.3	1.3	0.53	0.53
ϵ_e	4.4×10^{-3}	2.2×10^{-3}	1.1×10^{-2}	5.4×10^{-3}
ϵ_B	0.14	1.2×10^{-3}	0.01	$\sim 10^{-4}$

Table 6.3: Physical parameters estimated using the best fit spectral parameters mentioned in Table 6.2

6.5 Discussion

The collapse of a massive star is believed to be one of the probable progenitors of GRBs (Woosley, 1993). The association of a GRB with SN was first suspected in the case of GRB 980425 (Galama et al., 1999) because the error circle of the GRB location coincided with that of SN1998bw. Recently, the suspected association has been dramatically confirmed for GRB 030329 (Stanek et al., 2003) and for a few other GRBs. See e.g.,Woosley and Bloom (2006) and references therein. Thus, there is a mounting evidence, at least in the case of low redshift GRBs, for massive stars being progenitors of long GRBs. It is also well established that the massive stars lose significant fraction of their mass due to winds which they drive during their life time and modify the circum-stellar density profile in the process. The evolution of the GRB afterglows depends on the circum-burst medium and since GRBs are also due to massive star collapse it is imperative to study the circum-burst medium density profile to understand the GRB progenitors.

6.5.1 Stellar winds due to massive stars and the circum-stellar density profile

Observations have shown that the massive early type stars have stellar winds launched into the circum-burst medium with velocities of the order of $V \approx 1000$ km s^{-1} and mass loss rates $\dot{M} \approx 10^{-6} M_{\odot}$ yr^{-1}. These high velocity winds create a cavity in the circum-burst medium known as “Stellar Wind Bubble" bounded by a forward moving shock wave which propagates into the ISM and a backward moving shock wave i.e. a reverse shock that propagates into the wind. Morphology and evolution of the wind bubbles thus formed has been studied by Castor et al. (1975); Weaver et al. (1977). A reverse shock forms at the surface where the stellar wind meets the surrounding ISM and it then propagates into the wind. The free wind (upstream of the reverse shock) has a density profile $\rho \propto r^{-2}$ and the shocked wind (downstream of the reverse shock) has a constant density profile. Thus, the circum-burst medium around a massive star has four zones as illustrated graphically in Figure 6.3 and Figure 6.4, both taken from Weaver et al. (1977) [a] unshocked stellar wind, [b] stellar wind shocked by the reverse shock, [c] a thin shell consisting of shocked ISM and [d] unshocked ISM.

6.5.2 Signature of Wind Reverse Shock ?

The effects of such a density transition on the dynamics of blast wave has been investigated by Pe'er and Wijers (2006). It could be this transition of the density profile that we are observing at 0.02 day in the present case of GRB 050319. From the observations of long GRB afterglows, it has been inferred that most of the GRBs occur in constant density environment and the absence of wind signatures in the GRB afterglow was surprising. Various ways which can bring the wind reverse shock closer to the exploding star have recently been proposed to resolve this mystery

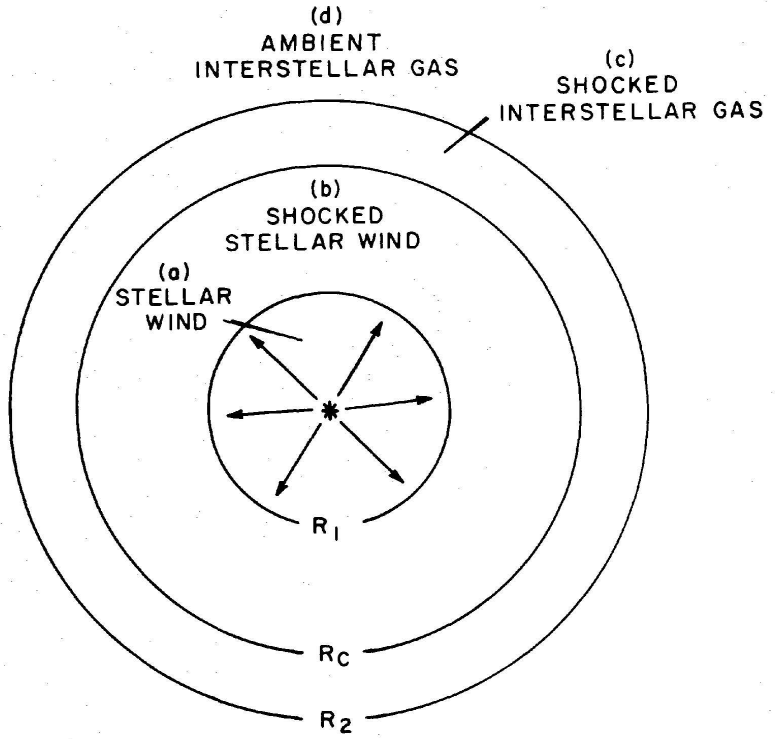

Figure 6.3: Schematic sketch indicating the regions and boundaries of the flow. From Weaver et al. (1977)

surrounding the absence of winds (van Marle et al., 2006; Eldridge, 2007). Notable among these are :

Low metalicity progenitors : Low metalicity of massive stars means low mass loss rate and hence low ram pressure which in turn can bring the wind termination shock closer to the progenitor star. Low metalicity for GRB progenitors has indeed been inferred from observations.

High-density ISM : If the density of the circum-stellar medium is high, the resulting wind-bubble would be smaller.

High-pressure ISM : This counter pressure can constrain the boundaries of the expanding wind-bubble. Examples of such an ISM are H II regions created by

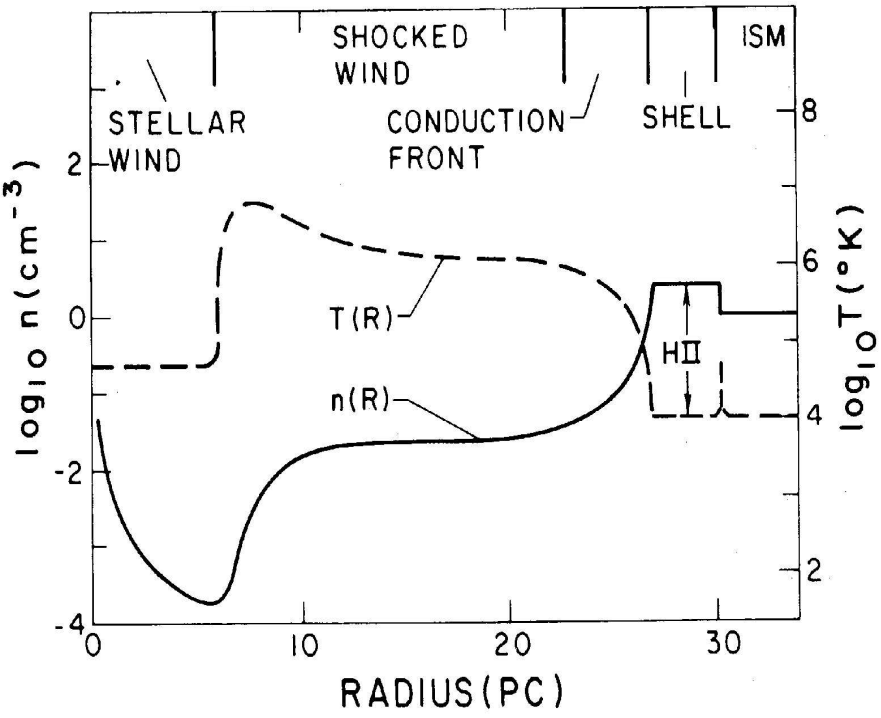

Figure 6.4: The large scale features of the temperature and density structure of an interstellar bubble for which $L_w = 1.27 \times 10^{36}$ ergs $s^{-1}, n_0 = 1$ cm^{-3}, and $t = 10^6$ yr. ISM means ambient interstellar medium. For a typical O7 I star, the H II region would extend to $\sim 3\ R_2$. From Weaver et al. (1977).

photo-ionization of the circum-stellar medium by the massive star.

Stellar motion : A progenitor star moving supersonically in the ISM can lead to a smaller radius of wind termination shock.

These scenarios and their combinations provide plausible explanations for smaller size wind bubbles and hence for the non-detection of the wind modified circum-burst medium in GRB afterglows.

In the case of GRB 050319, for a range of assumed values of $n = 1$ *to* 100, we estimate the radius of the reverse shock to be $R_{SW} \sim 0.5$ pc to 0.1 pc comparable to the values obtained by Eldridge (2006). The constraint $\epsilon_B < 1$ puts a lower bound

on density : $n > 0.03$ which is consistent with the values expected in the stellar wind bubbles (Castor et al., 1975; Weaver et al., 1977).

6.5.3 Implications for the models of GRB progenitors

The confirmation of GRB-SN association has provided a direct evidence of the massive stars indeed being the progenitors of the GRBs though the winds associated with them have not been detected. Our interpretation of the afterglow of GRB 050319 as being due to the wind-constant density transition supports the collapsar model of GRBs. This detection was made possible chiefly because of the quick follow up abilities of the robotic telescopes RAPTOR (Woźniak et al., 2005) and ROTSE-III (Quimby et al., 2006) coupled with those of *Swift* XRT (Cusumano et al., 2006) and UVOT (Mason et al., 2006).

The GRB-SN association is difficult to see in distant GRBs as the associated SN would be quite faint at that distance. As a result, this association has been confirmed only for low redshift GRBs. The circum-burst density transition, as seen in the present case of GRB 050319, can provide an alternative observational test of the progenitor for distant GRBs. The time dilation due to cosmological redshift delays the occurrence of the transition in the observer's frame of reference and makes it favourable to detect such a transition in distant GRBs. It is therefore necessary to carefully analyse multiband observations of distant GRBs to look for more examples of similar transition.

6.6 Summary

We have modeled the multiband afterglow of GRB 050319, using our own optical observations and other observations available in the literature, as being due to the interaction of the relativistic blast wave with circum-burst medium which shows a

transition of density profile from wind to constant density. Our conclusions can be summarised as follows :

1. We showed that the unusual break in the light curves of optical afterglow at 0.02 day can be explained as being due to the transition of circum-burst density profile from wind to constant density. The observed x-ray afterglow light curve without a simultaneous break is consistent with this interpretation. The overall afterglow can be explained by using a relatively low value of electron energy distribution index p which is also consistent with the x-ray spectral photon index.

2. The transition of the density profile could be due to the wind reverse shock propagating into the stellar wind driven by the progenitor of GRB 050319. We estimate the radius of the wind reverse shock to be $R_{SW} \sim 0.5\ pc\ to\ 0.1\ pc$ for assumed values of $n \sim 1\ to\ 100\ \mathrm{cm}^{-3}$ respectively.

Bibliography

Bessell M.S., Castelli F. and Plez B. A&A, 333, 231 (1998).

Castor J., McCray R. and Weaver R. ApJ Lett, 200, L107 (1975).

Chevalier R.A. and Li Z.Y. ApJ, 536, 195 (2000).

Cusumano G., Mangano V., Angelini L. et al. ApJ, 639, 316 (2006).

Eldridge J.J. ArXiv Astrophysics e-prints (2006).

Eldridge J.J. ArXiv Astrophysics e-prints (2007).

Fynbo J.P.U., Hjorth J., Jensen B.L. et al. GRB Coordinates Network, 3136, 1 (2005).

Galama T.J., Vreeswijk P.M., van Paradijs J. et al. A&AS, 138, 465 (1999).

Gendre B., Galli A., Corsi A. et al. A&A, 462, 565 (2007).

Henden A. GRB Coordinates Network, 3454, 1 (2005).

Huang K.Y., Urata Y., Kuo P.H. et al. ApJ Lett, 654, L25 (2007).

Krimm H., Sakamoto T., Barthelmy S. et al. GRB Coordinates Network, 3119, 1 (2005a).

Krimm H., Still M., Barthelmy S. et al. GRB Coordinates Network, 3117, 1 (2005b).

Mason K.O., Blustin A.J., Boyd P. et al. ApJ, 639, 311 (2006).

Mathis J.S. ARA&A, 28, 37 (1990).

Nousek J.A., Kouveliotou C., Grupe D. et al. ApJ, 642, 389 (2006).

Pe'er A. and Wijers R.A.M.J. ApJ, 643, 1036 (2006).

Quimby R.M., Rykoff E.S., Yost S.A. et al. ApJ, 640, 402 (2006).

Rykoff E., Schaefer B. and Quimby R. GRB Coordinates Network, 3116, 1 (2005).

Sari R., Narayan R. and Piran T. ApJ, 473, 204 (1996).

Sari R., Piran T. and Narayan R. ApJ Lett, 497, L17+ (1998).

Schlegel D.J., Finkbeiner D.P. and Davis M. ApJ, 500, 525 (1998).

Soderberg A.M. GRB Coordinates Network, 3127, 1 (2005a).

Soderberg A.M. GRB Coordinates Network, 3132, 1 (2005b).

Stanek K.Z., Matheson T., Garnavich P.M. et al. ApJ Lett, 591, L17 (2003).

van Marle A.J., Langer N., Achterberg A. and Garcaía-Segura G. A&A, 460, 105 (2006).

Volvach A. and Pozanenko A. GRB Coordinates Network, 3153, 1 (2005).

Weaver R., McCray R., Castor J., Shapiro P. and Moore R. ApJ, 218, 377 (1977).

Wijers R.A.M.J. and Galama T.J. ApJ, 523, 177 (1999).

Woosley S.E. ApJ, 405, 273 (1993).

Woosley S.E. and Bloom J.S. ARA&A, 44, 507 (2006).

Woźniak P.R., Vestrand W.T., Wren J.A. et al. ApJ Lett, 627, L13 (2005).